PCCP

ROYAL SOCIETY OF CHEMISTRY

PAPER

View Article Online
View Journal | View Issue



Cite this: *Phys. Chem. Chem. Phys.*, 2026, **28**, 12887

# *In vivo* 2D-IR spectroscopy of [NiFe] hydrogenases: a shielding role of the protein matrix

Mathesh Vaithiyanathan,[a] Cornelius C. M. Bernitzky,[a] Denise Poire,[ab] Janna Schoknecht,[c] Igor V. Sazanovich,[d] Partha Malakar,[d] Ryan Phelps,[d] Paul M. Donaldson,[d] Gregory M. Greetham,[d] Ingo Zebger,[c] Oliver Lenz[c] and Marius Horch*[a]

Received 20th February 2026,
Accepted 2nd May 2026

DOI: 10.1039/d6cp00618c

rsc.li/pccp

Hydrogenases are metalloenzymes that catalyze the cleavage and evolution of dihydrogen ($H_2$), a perfectly clean fuel. Thus, they represent ideal model catalysts for sustainable energy conversion approaches utilizing $H_2$. Due to the presence of biologically uncommon CO and $CN^-$ ligands at their catalytic metal sites, infrared (IR) spectroscopy is a key technique in hydrogenase research that can even be used to study these enzymes within living cells. Here, we introduce two-dimensional (2D) IR spectroscopy as a new *in vivo* technique for exploring the impact of the conditions in the cytoplasm on the properties of hydrogenases. Utilizing the soluble $NAD^+$-reducing [NiFe] hydrogenase from the $H_2$-oxidizing model bacterium *Cupriavidus necator* H16 as a suitable and biotechnologically relevant model enzyme, we demonstrate the feasibility of this approach. Our data indicates that even subtle structural details of the [NiFe] active site are unaffected by the unique gel-like properties of the highly dense cytoplasm, pointing towards a shielding role of the protein matrix that isolates this deeply buried metal center from environmental influences. In a more general sense, this study demonstrates that adequate strategies for scatter suppression can turn 2D-IR spectroscopy into a suitable technique for probing enzymes and other molecular targets in living cells and other complex biological environments.



## Introduction

The energy metabolism of many organisms involves hydrogenases, metalloenzymes that catalyze the reversible splitting of molecular hydrogen ($H_2$) into protons and electron.[1] This fundamental process is of significant importance as it can be emulated for the sustainable utilization of $H_2$ as a fuel or a source of reducing equivalents for biosynthesis.[1,2] In this context, $O_2$-tolerant $NAD^+$-reducing [NiFe] hydrogenases are valuable model enzymes, and whole-cell catalytic systems involving such enzymes promise to accomplish $H_2$-based processes in a truly sustainable manner. To tailor or enhance the efficiency of these processes however, a deep understanding of the *in vivo* properties of hydrogenases is required.

Infrared (IR) spectroscopy is a powerful technique for studying the active site of hydrogenases *via* the structurally sensitive stretching vibrations of intrinsic CO and $CN^-$ ligands bound to the active-site Fe (Fig. 1). Utilizing the soluble $NAD^+$-reducing [NiFe] hydrogenase from *Cupriavidus necator* H16 (*Cn*SH) as a model enzyme (Fig. 1), we have previously demonstrated that this technique can also be used to probe the [NiFe] active site *in vivo* (Fig. 2A).[3,4] Moreover, we have recently introduced two-dimensional (2D) IR spectroscopy as a novel technique for studying the structure and dynamics of hydrogenases in detail.[5–9] Here, we combine these two approaches to demonstrate how 2D-IR spectroscopy can be used to study hydrogenases in their native cellular environment. Utilizing the extraordinary sensitivity of this technique towards details of the solvent environment, we explore the impact of the cytoplasm on the active site by comparing spectra recorded from *Cn*SH in living cells of *C. necator* with those obtained from the isolated enzyme in dilute aqueous solution, poised in its catalytically active states. Our results indicate that the protein-embedded [NiFe] active site is effectively shielded from environmental solvent influences, *e.g.* those associated with altered water dynamics and macromolecular crowding in cells,[10,11] thereby supporting the idea of a protein scaffold that constrains the structure and dynamics of the catalytic center.[9,12–14] In a wider sense, this study illustrates that *in vivo* 2D-IR spectroscopy is a promising approach for studying enzymes and other molecular targets within complex environments like live cells.

[a] *Freie Universität Berlin, Department of Physics, Ultrafast Dynamics in Catalysis, Arnimallee 14, 14195, Berlin, Germany. E-mail: marius.horch@fu-berlin.de*
[b] *Technische Universität Berlin, Department of Chemistry, Modelling of Biomolecular Systems, Straße des 17. Juni 135, 10623, Berlin, Germany*
[c] *Technische Universität Berlin, Department of Chemistry, Sekr. PC14, Straße des 17. Juni 135, 10623, Berlin, Germany*
[d] *STFC Central Laser Facility, Research Complex at Harwell, Rutherford Appleton Laboratory, Harwell Campus, Didcot, OX11 0QX, UK*

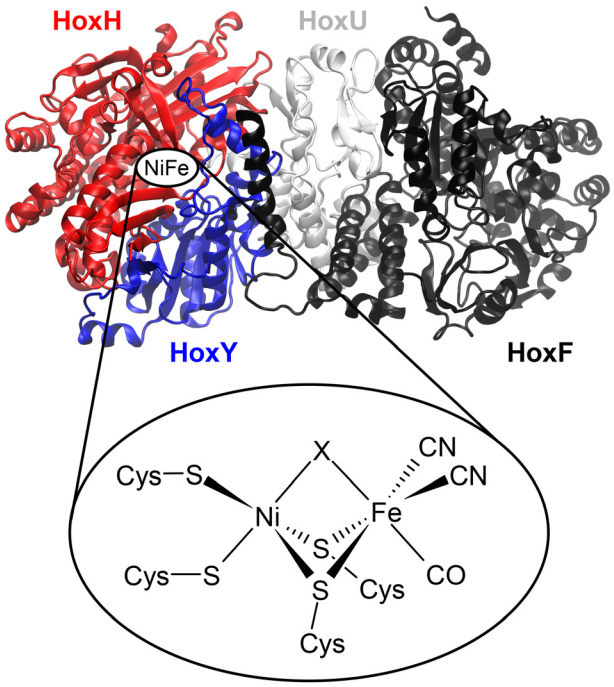


Fig. 1 Overall architecture of *Cn*SH and general structure of the [NiFe] active site. *Cn*SH is a dimodular enzyme consisting of the hydrogenase module, HoxHY (in red and blue), and a $NAD^+$ reductase (diaphorase) module, HoxFU (in black and white). The [NiFe] active site is located in the hydrogenase large subunit, HoxH (in red), close to the interface with the small hydrogenase subunit, HoxY (in blue). The general structure and localization of the [NiFe] site is conserved in all [NiFe] hydrogenases. The homology model of heterotetrameric *Cn*SH was generated using AlphaFold2.[23]

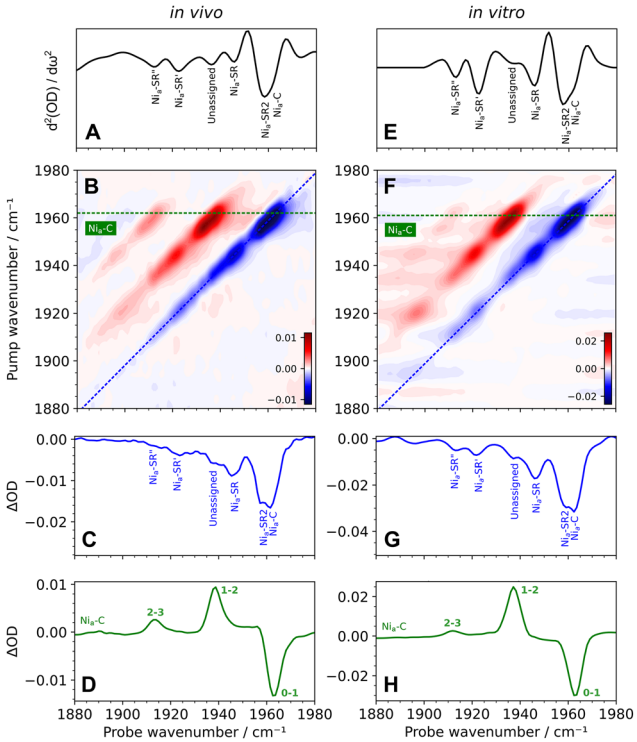


Fig. 2 IR spectroscopic signatures of *Cn*SH in living cells of *C. necator* (*in vivo*, left) and as purified, NADH-reduced protein (*in vitro*, right). From top to bottom: (A and E) Linear IR absorption spectra, represented as second derivatives. (B and F) 2D-IR spectra shown as contour plots. (C and G) Diagonal slices through the 2D-IR spectra. (D and H) Pump slices through the 2D-IR spectra, exemplarily shown for the $Ni_a$-C state. The positions of the diagonal slices and the pump slices are shown in panels B and F as dotted blue and green lines, respectively. 2D-IR spectra were recorded at a waiting time of $T_W$ = 250 fs with parallel pump–probe polarization and interpolated as described in the Supplementary Information. Non-interpolated data are shown in Fig. S4.

## Results and discussion

*In vivo* IR spectroscopy on enzymes usually poses inherent challenges, primarily stemming from the lack of contrast against the cellular background, including other proteins, and the low concentration of the target molecule within the cytoplasm (number of molecules per unit cytoplasm volume). The latter issue is enhanced by finite cell densities, which further reduce the effective enzyme concentration (number of molecules per unit sample volume). Here, we address these challenges in three ways. (1) The lack of contrast can be circumvented by using appropriate IR chromophores, either artificially introduced or inherent to the target system. [NiFe] hydrogenases represent ideal model systems in this regard as their intrinsic CO and CN oscillators absorb in a spectral region (1900 and 2100 $cm^{-1}$) that is free from other cellular contributions and barely affected by water absorption. (2) Low cellular enzyme concentrations can be overcome by high expression levels. Due to a mutation in a hydrogenase regulatory gene of wild-type *C. necator*, the intracellular *Cn*SH concentration can be very high even in the absence of $H_2$,[15,16] and cytoplasmic concentrations of this enzyme can be further increased by homologous overproduction without affecting the vitality of the cells.[3,17] (3) The overall enzyme concentration can be additionally raised by concentrating *C. necator* cell suspensions to high densities, as previously demonstrated.[3] The latter strategy not only increases the effective sample concentration without altering intracellular concentrations but also reduces the water content of the samples, which is advantageous for 2D-IR spectroscopy, where water absorption of pump and probe light adversely affects signal size and noise. We like to stress that the conditions used here do not impair the vitality of the cells. The intracellular concentration of *Cn*SH is naturally high under the chosen growth conditions, and *C. necator* H16 has been described as a biofilm-producing soil bacterium.[18] This means that it can thrive in high-density cell aggregates, similar to the high cell densities used here for the spectroscopic experiments.

While the structure and dynamics of synthetic peptides have been studied by 2D-IR spectroscopy under conditions mimicking the cellular environment,[19,20] studies on proteins inside living cells are scarce. The only published example is the investigation of CO-bound hemoglobin in erythrocytes,[21,22] which was possible due to the exceptionally high hemoglobin concentration of up to 96% of the cell dry weight.[23] Such high intracellular concentrations are non-physiological and unattainable for the vast majority of proteins and therefore mimic the situation in

concentrated solutions of isolated proteins rather than that found in cells. To the best of our knowledge, no 2D-IR studies have been conducted on typical eukaryotic cells or prokaryotic cells, and, furthermore, no enzyme has been studied *in vivo* by 2D-IR spectroscopy.

One of the key challenges in the application of 2D-IR spectroscopy *in vivo* is the occurrence of strong diagonal artifacts due to pump-light scattering by cell suspensions (see Fig. S1). Scattering can be mitigated through a combination of (1) probe chopping,[20] (2) polarization control, (3) careful subtraction of negative time delays,[21] (4) phase cycling, and (5) the utilization of a bright probe beam.[22] Probe chopping (1) is avoided here as it introduced disproportionate amounts of noise on our setup. The use of a perpendicular pump–probe polarization geometry $\langle ZZXX \rangle$ (2) eliminates the scattering effect on diagonal signals but also reduces their intensity. Subtraction of negative time delays (3) was unable to remove scattering contributions in the current case. To avoid the limitations of (1) and (2) and retain the additional information available from polarization-resolved experiments, we focus on the following two approaches: (4) Usage of four-frame phase cycling, which is based on the summation of data obtained with different phase relations between the two pump pulses in a way that retains the 2D-IR signals and cancels scattering contributions. (5) Utilization of a bright probe as an easy and straightforward method to obtain a better signal-to-noise ratio and, in particular, reduce scattering contributions.[22] Fig. 2B shows a 2D-IR spectrum of the CO stretching region of *Cn*SH in intact cells obtained with parallel pump–probe polarization $\langle ZZZZ \rangle$ by combining four-frame phase cycling and a bright probe beam. The spectrum is almost free of scattering contributions as can be seen from the absence of interfering intensity along the diagonal (*cf.* Fig. S1). In addition, the spectrum reveals all expected signals in the probed spectral region, as discussed below, demonstrating the possibility to obtain high-quality 2D-IR spectra of hydrogenases *in vivo*. This is further supported by the observation of weaker signals related to the CN stretching vibrations (Fig. S2). Due to their small transition dipole moments and the high spectral complexity related to at least eight overlapping peaks in the 2D-IR spectrum of each probed [NiFe] state,[6,7] these vibrational modes are generally less suited for analyses of complex catalytic mixtures, as observed *in vivo*. We also note that the CO ligand is positioned *trans* to the substrate binding site of [NiFe] hydrogenases and most relevant for controlling $H_2$ activation and cleavage, due to its Lewis amphoteric character. For these reasons, we will focus on the more intense and less congested CO stretching region of the 2D-IR spectrum and the properties of the CO ligand in the following.

We start our analysis by comparing linear IR and 2D-IR spectra *in vivo*. Different redox-structural states of the [NiFe] active site are best identified by their characteristic CO stretching vibrations (*ca.* 1900–2000 $cm^{-1}$). These fundamental ($0 \rightarrow 1$) transitions can be detected by linear IR spectroscopy or observed as diagonal signals in the 2D-IR spectrum. Comparing the diagonal slice of the *in vivo* 2D-IR spectrum (Fig. 2C and Fig. S3) with the linear *in vivo* IR spectrum (Fig. 2A), the diagonal features of the 2D-IR spectrum reproduce the composition of catalytic states discerned through linear IR absorption spectroscopy. In addition, the observed *in vivo* composition is similar to previous observations from *C. necator* cells.[3] Specifically, the peaks at approximate positions of 1962, 1957, 1946, 1937, and 1926 $cm^{-1}$ signify the presence of the catalytic intermediate $Ni_a$-C, the unique $Ni_a$-SR2 state, the reduced $Ni_a$-SR state, an unassigned but previously observed species,[3,4] and the $Ni_a$-SR′ state, respectively.[3] An additional signal can be observed around 1912 $cm^{-1}$, indicating the presence of the $Ni_a$-SR″ state, but the intensity is too low for proper fitting. This ensemble of catalytic states is also similar to the mixture observed for purified, NADH-reduced *Cn*SH (Fig. 2E–G). In the following, we will therefore compare the *in vivo* 2D-IR spectrum of *Cn*SH in intact *C. necator* cells with the corresponding *in vitro* spectrum recorded from the reduced enzyme (Fig. 2B and F).

The visual comparison of *in vivo* and *in vitro* 2D-IR spectra of *Cn*SH reveals striking similarities in terms of frequencies, relative intensities, and two-dimensional lineshapes for all observed signals in the CO stretch region. Specifically, $Ni_a$-C, $Ni_a$-SR2, $Ni_a$-SR, the above-mentioned unassigned state, and $Ni_a$-SR′ are observed as diagonal signals at fundamental frequencies of *ca.* 1961, 1957, 1945, 1936, and 1921 $cm^{-1}$ in the *in vitro* 2D-IR spectrum of *Cn*SH. In addition, the $Ni_a$-SR″ state, which is not clearly discernible in the *in vivo* 2D-IR spectrum of *Cn*SH, is well-resolved in the *in vitro* 2D-IR spectrum of the isolated enzyme at 1911 $cm^{-1}$. Inspecting diagonal cuts of the two 2D-IR spectra, we further note similar relative intensities in the *in vitro* and *in vivo* data, in line with the linear IR spectra. As observed previously, $Ni_a$-SR″ exhibits the lowest relative intensity among all reduced states, which explains why it is not well resolved in the *in vivo* 2D-IR spectrum. In total, similar fundamental $E_{0\rightarrow1}$ transition energies and associated line intensities are observed for *Cn*SH *in vitro* and *in vivo*, indicating that the equilibrium structure of the [NiFe] active site is not significantly affected by the (cytoplasmic) solvent environment of *Cn*SH, which is consistent with previous linear IR studies.[3,24]

Next, we inspect excited-state absorption energies ($E_{1\rightarrow2}$ and $E_{2\rightarrow3}$) that can be extracted from (horizontal) pump slices through the 2D-IR spectrum, as demonstrated for the $Ni_a$-C state (Fig. 2D and H and Fig. S5).[5,9] These observables, which provide insights into the shape of the potential energy surface and the bond properties of the CO ligand, are not accessible by linear IR spectroscopy but well studied by 2D-IR spectroscopy of hydrogenases.[5–9] Excited-state absorption energies extracted from *in vivo* and *in vitro* 2D-IR spectra of *Cn*SH are listed in Table S1 for all detectable [NiFe] states together with the corresponding anharmonicities. The latter quantities are calculated as differences between subsequent vibrational transition energies, *e.g.* $E_{0\rightarrow1} - E_{1\rightarrow2}$. Thus, they represent powerful descriptors reflecting the shape of the CO bond potential, robust against possible systematic errors in wavenumber accuracy. For an idealized Morse oscillator (diatomic molecule in the gas phase), the difference between neighboring transition energies ($E_{0\rightarrow1}$, $E_{1\rightarrow2}$, and $E_{2\rightarrow3}$) is a constant. Inspecting the obtained anharmonicities, we find no significant differences between *Cn*SH in *C. necator* cells and the isolated enzyme that are conserved across all redox-structural states (Fig. 3A). In both

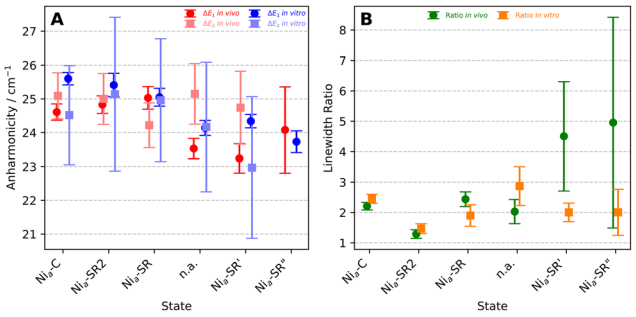


Fig. 3 Comparison of key quantities extracted from *in vivo* and *in vitro* 2D-IR spectra of *Cn*SH. (A) Anharmonicities $\Delta E_1 = E_{0\to1} - E_{1\to2}$ and $\Delta E_2 = E_{1\to2} - E_{2\to3}$. (B) Linewidth ratio (diagonal/antidiagonal) of the peak corresponding to the $E_{0\to1}$ transition. Data are shown for all probed redox-structural states of the [NiFe] centre. Error bars reflect the uncertainties of the plotted quantitates, calculated from the standard errors of the fitting procedures used to determine transition energies and linewidths (also see Fig. S5 as well as Tables S1 and S2).

cases, the observed transition energies approximate the behavior expected for an idealized Morse oscillator, consistent with our previous 2D-IR studies on other [NiFe] hydrogenases.[5,6,9] As a consequence, the CO ligand can be described as a diatomic oscillator, and the associated bond properties of this ligand are experimentally indistinguishable for purified SH and the enzyme in the highly dense cytoplasm.

While absolute and relative transition energies of *Cn*SH are practically identical *in vivo* and *in vitro*, we note differences in relative intensities associated with the higher vibrational transitions. Despite the low overall concentration of *Cn*SH in the cell suspension, higher vibrational transitions, $E_{2\to3}$, which are generally less intense, are observed in the *in vivo* 2D-IR spectrum (Fig. 2B). This can be explained by higher relative intensities than those observed in the *in vitro* 2D-IR spectrum (Fig. 2D, H and Fig. S5). While it is tempting to ascribe this phenomenon to solvent-induced differences in the protein shell, it should be noted that the usage of a bright probe beam increases contributions of higher-order signals in the formally third-order 2D-IR spectrum.[22] Consistently, *in vivo* 2D-IR spectra recorded with a weak probe beam exhibit relative intensities that are comparable to those observed for the isolated enzyme (Fig. S6). While the observation of higher vibrational transitions is useful for mapping out vibrational bond potentials, the possibility of increased contributions from higher-order signals needs to be taken into account when recording *in vivo* 2D-IR spectra with a bright probe beam, in order to avoid misleading conclusions.

We next turn our attention to an analysis of the two-dimensional lineshapes of the 2D-IR spectra. As demonstrated previously, the total linewidths of CO and CN stretching vibrations of [NiFe] hydrogenases can be interpreted in terms of a narrow inhomogeneous distribution of structural microstates.[9] If such microstates interconvert on timescales that are compatible with those of the 2D-IR experiments, spectral diffusion might be observed as a waiting-time dependent change of the 2D lineshape.[25] At early waiting times between pump and probe events, the lineshape will be diagonally elongated, because microstates in resonance with a certain pump frequency will be probed at the same frequency, before converting into other microstates of the distribution that absorb at slightly different frequencies. In that case, the anti-diagonal linewidth reflects the homogeneous width governed by fast dynamics and ultimately limited by the vibrational lifetime. The diagonal linewidth, on the other hand, is a convolution of the homogenous and the inhomogeneous width, the latter reflecting the distribution of slowly-converting structural microstates. At later waiting times, 2D lineshapes will become more circular, because the entire inhomogeneous distribution is sampled by the infrared chromophore between pump and probe events. While 2D-IR signal intensities of *Cn*SH in living cells are too weak to be analyzed at later waiting times, the ratio of diagonal and antidiagonal linewidths at early waiting times provides valuable information on the width of the inhomogeneous distribution and the degree to which the underlying microstates might interconvert at ultrashort timescales. Analyzing these aspects by determining the full width at half maximum in both diagonal and anti-diagonal directions, we find no significant differences between the purified *Cn*SH and the enzyme in its native cellular environment (Fig. 3B and Table S2). More specifically, there is no systematic decrease or increase of the ratio between diagonal and antidiagonal linewidths that is conserved across the probed redox-structural states of the [NiFe] center. This outcome strongly suggests a scenario wherein the active site, which is deeply embedded in the enzyme, experiences minimal molecular interaction with the cellular solvent environment or the artificial solvent. This conclusion is in line with the previously deduced narrow distribution of structural microstates and their slow interconversion.[9]

In total, the comparison of *in vivo* and *in vitro* 2D-IR spectra of *Cn*SH has revealed remarkable similarities between the cytoplasmic enzyme and its purified counterpart, despite the inherent sensitivity of the CO/CN oscillators to environmental influences.[8] This is relevant for two reasons: (1) The fact that all spectroscopic observables are unaffected by the environment indicates that the [NiFe] site is well isolated from environmental (solvent) influences. This finding provides further support for the idea that the chelating amide scaffold and the active site cavity functionalize the [NiFe] site through a rigid framework, while the overall protein environment acts as an insulating shell that prevents severe effects of aqueous environments on the active site.[6–9,12–14] This key aspect of the enzyme's functionality has been overlooked in design strategies aiming at the creation of synthetic biomimetic catalysts for dihydrogen conversion. (2) The indistinguishability of *in vivo* and *in vitro* 2D-IR spectra indicates that biologically relevant information on the [NiFe] active site can be obtained by this technique from studies on purified enzymes. This finding allows detailed *in vitro* studies at high protein concentration and under precise experimental control that would be impossible to realize *in vivo*.

## Conclusion

In the current study, we have demonstrated how 2D-IR spectroscopy can be utilized to study hydrogenases within their cellular environment. This methodology promises representative insights

 

into the native structure and dynamics of hydrogenases, which is particularly relevant for the knowledge-based design of cellular systems for the evolution or utilization of dihydrogen. For the investigated model enzyme, the soluble $NAD^+$-reducing [NiFe] hydrogenase from *C. necator*, we find a remarkable similarity of *in vivo* and *in vitro* data. On the one hand, this finding highlights the role of the protein matrix as a functional scaffold that (1) creates an entatic state of the [NiFe] center and (2) isolates this catalytic site from the solvent environment. We propose that these aspects should be considered in the future design of bioinspired catalysts for dihydrogen conversion. On the other hand, it provides a solid basis for the more common approach of studying isolated hydrogenases in dilute aqueous solution. It remains to be tested whether the similarity of *in vivo* and *in vitro* properties extends to other types of hydrogenases, such as [FeFe] hydrogenases, whose active site has only a single covalent bond to the protein.

In a broader sense, the current study demonstrated the power of scatter suppression approaches[21,22] and the resulting feasibility of studying molecular targets by 2D-IR spectroscopy within live cells or other complex biological environments. Besides hydrogenases, this approach can be directly applied to other organometallic systems, *e.g.* CO-releasing molecules for therapeutic applications.[26] Even more, the utilization of non-canonical amino acids carrying suitable IR chromophores, *e.g.* thiocyanate or azide groups,[27–33] can extend this strategy towards various research questions and any desired protein synthesized within a genetically amenable organism. We therefore expect this approach to considerably broaden the scope of 2D-IR spectroscopy and its application within the molecular life sciences. It will be exciting to see how different cell types, intracellular composition, and localization in subcellular compartments affect the structure, function, and dynamics of different target molecules and their cofactors.

Mathesh Vaithiyanathan: data curation, formal analysis, investigation, methodology, software, validation, visualization, writing – original draft, writing – review & editing; Cornelius C. M. Bernitzky: investigation, writing – review & editing; Denise Poire: investigation, writing – review & editing; Janna Schoknecht: investigation, writing – review & editing; Igor V. Sazanovich: methodology, writing – review & editing; Partha Malakar: methodology, writing – review & editing; Ryan Phelps: methodology, writing – review & editing; Paul M. Donaldson: methodology, writing – review & editing; Gregory M. Greetham: methodology, software, writing – review & editing; Ingo Zebger: funding acquisition, resources, writing – review & editing; Oliver Lenz: funding acquisition, resources, writing – review & editing; Marius Horch: conceptualization, data curation, formal analysis, funding acquisition, investigation, methodology, project administration, supervision, validation, visualization, writing – original draft, writing – review & editing.

## Conflicts of interest

There are no conflicts to declare.

## Abbreviations

| | |
|---|---|
| 2D-IR | two-dimensional infrared. |
| [NiFe] | nikel-iron. |
| NAD | nicotinamide adenine dinucleotide. |
| *Cn*SH | *Cupriavidus necator* soluble hydrogenase. |

## Data availability

The data supporting this article have been included as part of the supplementary information (SI): Experimental details, Supplementary Figures, and Supplementary Tables. The authors have included the supporting information and have cited additional references within the supplementary information.[3,17,22,34–36] See DOI: https://doi.org/10.1039/d6cp00618c.

## Acknowledgements

This work was funded by the Deutsche Forschungsgemeinschaft (DFG, German Research Foundation) under Germany's Excellence Strategy – EXC 2008 – 390540038, UniSysCat (Unifying Systems in Catalysis). C. C. M. B., D. P., and M. H. are grateful for financial support by the Einstein Foundation Berlin. O. L. and I. Z. are thankful for financial support from EU Horizon 2020/McGEA/Proposal ID 101183014 HORIZON-MSCA-2023-SE-01-01. The authors thank the STFC for funding access to the ULTRA laser system at the STFC Central Laser Facility (23130006 and 24230005). The research leading to these results has received funding from LASERLAB-EUROPE (grant agreement no. 871124, European Union's Horizon 2020 research and innovation programme). The authors thank Dr Stefan Frielingsdorf for providing the homology model of *Cn*SH shown in Fig. 1 and Dr James Birrell for support during the experiments and helpful comments on the manuscript.

## References

1 R. Cammack, F. Michel and R. Robert, *Hydrogen as a fuel: learning from nature*, CRC Press, 2001, DOI: 10.1201/9780203471043.
2 L. Lauterbach, O. Lenz and K. A. Vincent, *FEBS J.*, 2013, **280**, 3058–3068.
3 M. Horch, L. Lauterbach, M. Saggu, P. Hildebrandt, F. Lendzian, R. Bittl, O. Lenz and I. Zebger, *Angew. Chem., Int. Ed.*, 2010, **49**, 8026–8029.
4 L. Lauterbach, J. Liu, M. Horch, P. Hummel, A. Schwarze, M. Haumann, K. A. Vincent, O. Lenz and I. Zebger, *Eur. J. Inorg. Chem.*, 2011, 1067–1079.
5 C. J. Kulka-Peschke, A. C. Schulz, C. Lorent, Y. Rippers, S. Wahlefeld, J. Preissler, C. Schulz, C. Wiemann, C. C. M. Bernitzky, C. Karafoulidi-Retsou, S. L. D. Wrathall, B. Procacci, H. Matsuura, G. M. Greetham, C. Teutloff, L. Lauterbach, Y. Higuchi, M. Ishii, N. T. Hunt, O. Lenz, I. Zebger and M. Horch, *J. Am. Chem. Soc.*, 2022, **144**, 17022–17032.

6 S. L. D. Wrathall, B. Procacci, M. Horch, E. Saxton, C. Furlan, J. Walton, Y. Rippers, J. N. Blaza, G. M. Greetham, M. Towrie, A. W. Parker, J. Lynam, A. Parkin and N. T. Hunt, *Phys. Chem. Chem. Phys.*, 2022, **24**, 24767–24783.
7 Y. Rippers, B. Procacci, N. T. Hunt and M. Horch, *Catalysts*, 2022, **12**, 988.
8 B. Procacci, S. L. D. Wrathall, A. L. Farmer, D. J. Shaw, G. M. Greetham, A. W. Parker, Y. Rippers, M. Horch, J. M. Lynam and N. T. Hunt, *J. Phys. Chem. B*, 2024, **128**, 1461–1472.
9 M. Horch, J. Schoknecht, S. L. D. Wrathall, G. M. Greetham, O. Lenz and N. T. Hunt, *Chem. Sci.*, 2019, **10**, 8981.
10 X. You and C. R. Baiz, *J. Phys. Chem. A*, 2022, **126**, 5881–5889.
11 L. Goett-Zink, J. L. Klocke, L. A. K. Bögeholz and T. Kottke, *J. Biol. Chem.*, 2020, **295**, 11729–11741.
12 M. Horch, J. Schoknecht, M. A. Mroginski, O. Lenz, P. Hildebrandt and I. Zebger, *J. Am. Chem. Soc.*, 2014, **136**, 9870–9873.
13 M. Bruschi, M. Tiberti, A. Guerra and L. De Gioia, *J. Am. Chem. Soc.*, 2014, **136**, 1803–1814.
14 Y. Ilina, C. Lorent, S. Katz, J. H. Jeoung, S. Shima, M. Horch, I. Zebger and H. Dobbek, *Angew. Chem., Int. Ed.*, 2019, **58**, 18710–18714.
15 M. Jahn, N. Crang, A. H. Gynnå, D. Kabova, S. Frielingsdorf, O. Lenz, E. Charpentier and E. P. Hudson, *Appl. Environ. Microbiol.*, 2024, **90**, e00748-24.
16 O. Lenz and B. Friedrich, *Proc. Natl. Acad. Sci. U. S. A.*, 1998, **95**, 12474–12479.
17 L. Lauterbach and O. Lenz, *J. Am. Chem. Soc.*, 2013, **135**, 17897–17905.
18 E. Wilde, *Arch. Mikrobiol.*, 1962, **43**, 109–137.
19 K. A. Lorenz-Ochoa and C. R. Baiz, *J. Am. Chem. Soc.*, 2023, **145**, 27800–27809.
20 C. R. Baiz, D. Schach, A. Tokmakoff, J. Manor, P. Mukherjee, Y. S. Lin, H. Leonov, J. L. Skinner, M. T. Zanni, I. T. Arkin, G. mechanism, A. Bakulin, C. Liang, T. la Cour Jansen, D. A. Wiersma, H. J. Bakker, M. S. Pshenichnikov, D. G. Kuroda, J. D. Bauman, J. R. Challa, D. Patel, T. Troxler, K. Das, E. Arnold and R. M. Hochstrasser, *Opt. Express*, 2014, **22**, 18724–18735.
21 A. M. Casas, N. S. Idris, V. Wen, J. P. Patterson and N. H. Ge, *J. Phys. Chem. B*, 2024, **128**, 8845.
22 P. M. Donaldson, R. F. Howe, A. P. Hawkins, M. Towrie and G. M. Greetham, *J. Chem. Phys.*, 2023, **158**, 114201.
23 J. Jumper, R. Evans, A. Pritzel, T. Green, M. Figurnov, O. Ronneberger, K. Tunyasuvunakool, R. Bates, A. Žídek, A. Potapenko, A. Bridgland, C. Meyer, S. A. A. Kohl, A. J. Ballard, A. Cowie, B. Romera-Paredes, S. Nikolov, R. Jain, J. Adler, T. Back, S. Petersen, D. Reiman, E. Clancy, M. Zielinski, M. Steinegger, M. Pacholska, T. Berghammer, S. Bodenstein, D. Silver, O. Vinyals, A. W. Senior, K. Kavukcuoglu, P. Kohli and D. Hassabis, *Nature*, 2021, **596**, 583–589.
24 M. Horch, L. Lauterbach, M. A. Mroginski, P. Hildebrandt, O. Lenz and I. Zebger, *J. Am. Chem. Soc.*, 2015, **137**, 2555–2564.
25 P. Hamm and M. T. Zanni, *Concepts and methods of 2D infrared spectroscopy*, Cambridge University Press, 2011.
26 M. Klein, U. Neugebauer, A. Gheisari, A. Malassa, T. M. A. Jazzazi, F. Froehlich, M. Westerhausen, M. Schmitt and J. Popp, *J. Phys. Chem. A*, 2014, **118**, 5381–5390.
27 J. M. Schmidt-Engler, R. Zangl, P. Guldan, N. Morgner and J. Bredenbeck, *Phys. Chem. Chem. Phys.*, 2020, **22**, 5463–5475.
28 M. C. Thielges, J. Y. Axup, D. Wong, H. S. Lee, J. K. Chung, P. G. Schultz and M. D. Fayer, *J. Phys. Chem. B*, 2011, **115**, 11294–11304.
29 E. Deniz, L. Valiño-Borau, J. G. Löffler, K. B. Eberl, A. Gulzar, S. Wolf, P. M. Durkin, R. Kaml, N. Budisa, G. Stock and J. Bredenbeck, *Nat. Commun.*, 2021, **12**, 1–8.
30 K. B. Eberl, H. M. Müller-Werkmeister, M. Essig and J. Bredenbeck, *Biophys. J.*, 2015, **108**, 185a.
31 L. J. G. W. Van Wilderen, D. Kern-Michler, H. M. Müller-Werkmeister and J. Bredenbeck, *Phys. Chem. Chem. Phys.*, 2014, **16**, 19643–19653.
32 J. M. Schmidt-Engler, L. Blankenburg, B. Błasiak, L. J. G. W. Van Wilderen, M. Cho and J. Bredenbeck, *Anal. Chem.*, 2019, **92**, 1024–1032.
33 J. M. Schmidt-Engler, L. Blankenburg, R. Zangl, J. Hoffmann, N. Morgner and J. Bredenbeck, *Phys. Chem. Chem. Phys.*, 2020, **22**, 22963–22972.
34 A. Tokmakoff, L. P. DeFlores and R. A. Nicodemus, *Opt. Lett.*, 2007, **32**, 2966–2968.
35 S. H. Shim, D. B. Strasfeld, Y. L. Ling and M. T. Zanni, *Proc. Natl. Acad. Sci. U. S. A.*, 2007, **104**, 14197–14202.
36 Y. Feng, I. Vinogradov, N.-H. Ge, W. S. Chan and T. K. Yee, *Opt. Express*, 2017, **25**, 26262–26279.

 